

# Correlating Photoacidity to Hydrogen-Bond Structure by Using the Local O–H Stretching Probe in Hydrogen-Bonded Complexes of Aromatic Alcohols

Brian T. Psciuk,<sup>†</sup> Mirabelle Prémont-Schwarz,<sup>‡</sup> Benjamin Koeppe,<sup>‡</sup> Sharon Keinan,<sup>§</sup> Dequan Xiao,<sup>||</sup> Erik T. J. Nibbering,<sup>\*,‡</sup> and Victor S. Batista<sup>\*,†</sup>

<sup>†</sup>Department of Chemistry, Yale University, 225 Prospect Street, New Haven, Connecticut 06520, United States

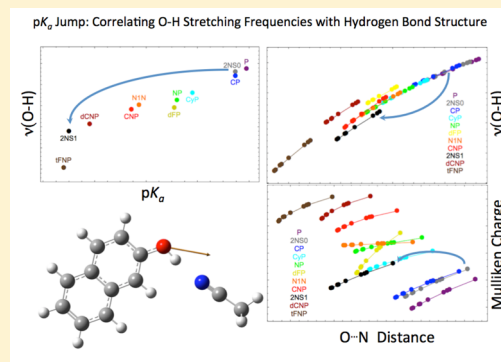
<sup>‡</sup>Max Born Institut für Nichtlineare Optik und Kurzzeitspektroskopie, Max Born Strasse 2A, D-12489 Berlin, Germany

<sup>§</sup>Department of Chemistry, Ben-Gurion University of the Negev, P.O. Box 653, Be'er Sheva, 84105, Israel

<sup>||</sup>Department of Chemistry & Chemical Engineering, University of New Haven, 300 Boston Post Road, West Haven, Connecticut 06516, United States

## Supporting Information

**ABSTRACT:** To assess the potential use of O–H stretching modes of aromatic alcohols as ultrafast local probes of transient structures and photoacidity, we analyze the response of the O–H stretching mode in the 2-naphthol-acetonitrile (2N–CH<sub>3</sub>CN) 1:1 complex after UV photoexcitation. We combine femtosecond UV-infrared pump–probe spectroscopy and a theoretical treatment of vibrational solvatochromic effects based on the Pullin perturbative approach, parametrized at the density functional theory (DFT) level. We analyze the effect of hydrogen bonding on the vibrational properties of the photoacid–base complex in the S<sub>0</sub> state, as compared to O–H stretching vibrations in a wide range of substituted phenols and naphthols covering the 3000–3650 cm<sup>−1</sup> frequency range. Ground state vibrational properties of these phenols and naphthols with various substituent functional groups are analyzed in solvents of different polarity and compared to the vibrational frequency shift of 2N induced by UV photoexcitation to the <sup>1</sup>L<sub>b</sub> electronic excited state. We find that the O–H stretching frequency shifts follow a linear relationship with the solvent polarity function  $F_0 = (2\epsilon_0 - 2)/(2\epsilon_0 + 1)$ , where  $\epsilon_0$  is the static dielectric constant of the solvent. These changes are directly correlated with photoacidity trends determined by reported pK<sub>a</sub> values and with structural changes in the O⋯N and O–H hydrogen-bond distances induced by solvation or photoexcitation of the hydrogen-bonded complexes.



## INTRODUCTION

Determination of the microscopic nature of the reaction coordinate is a prerequisite for understanding the outcome of a chemical reaction. For this, not only the molecular degrees of freedom of the reactants and products are important but also a mapping of the energy pathways including the important roles of the surrounding solvent. For proton transfer dynamics, one has to characterize the hydrogen bond connecting acid and base molecules in real-time. Hydrogen bond structures have been investigated for many decades by using crystallographic,<sup>1</sup> thermodynamic,<sup>2</sup> and spectroscopic methods.<sup>3,4</sup> Trends in hydrogen bonding interactions with electrostatic, covalent, and charge transfer contributions, and trends in proton affinities and acidities (pK<sub>a</sub> values) have been correlated to interatomic distances obtained from diffraction techniques and spectroscopic observables probing electronic, vibrational or spin degrees of freedom.<sup>5–7</sup> Those studies have led to widely used empirical correlations of hydrogen bond distances with IR-active vibrational mode transition frequencies.<sup>8–12</sup> These

steady-state techniques provide only time-averaged insight into structures equilibrated in the electronic ground state. Resolving the underlying microscopic mechanisms for proton transfer dynamics requires methods with structure determination capabilities combined with temporally resolved spectroscopy. The development of new methods for ultrafast studies of structural dynamics<sup>13,14</sup> will ultimately be highly beneficial for condensed-phase charge transfer studies, ranging from electron donor–acceptor systems to aqueous proton transfer and proton-coupled electron transfer in energy conversion systems.<sup>15–17</sup>

For time-resolved proton transfer studies, photoacid molecules are particularly useful.<sup>18–22</sup> Photoacids exhibit a large jump in acidity upon S<sub>0</sub> → S<sub>1</sub> electronic excitation as exemplified by a change in acidity of  $\Delta pK_a = pK_a(S_1) -$

Received: February 13, 2015

Revised: April 16, 2015

$pK_a(S_0) \approx 5-12$ .<sup>23,24</sup> For instance, free-energy reactivity correlations of photoacids have been reported showing the close connection between changes in  $pK_a$  values and proton transfer rates.<sup>25,26</sup> Moreover, using femtosecond mid-infrared spectroscopy on photoacids, it has been possible to obtain unprecedented dynamical detail on the possible reaction pathways in aqueous acid–base neutralization reactions.<sup>27–29</sup> Despite the richness in kinetic details revealed by studies of aqueous proton transfer pathways, a microscopic characterization of the hydrogen bond reaction coordinate associated with photoacidity remains a topic of intense research.<sup>30–38</sup> The characterization of hydrogen bond structures in both the  $S_0$  and  $S_1$  states could provide valuable insights on the molecular origin of photoacidity, since minor electronic changes affect the photoacid side while more significant electronic changes have been reported for the photobase side of the Förster cycle.<sup>30,31,39</sup>

Here, we present a study of the hydrogen bond of a photoacid–base pair in solution with a combined experimental and theoretical approach using ultrafast mid-IR spectroscopy and time-dependent density functional theory (TD-DFT) quantum chemical calculations. We study the solvent-dependent frequency shifts of the O–H stretching mode of a prototypical photoacid, 2-naphthol (Figure 1), as a local probe of the hydrogen bond with acetonitrile in the electronic ground and first excited states. We chose acetonitrile as hydrogen bond acceptor for the following reasons: (a)

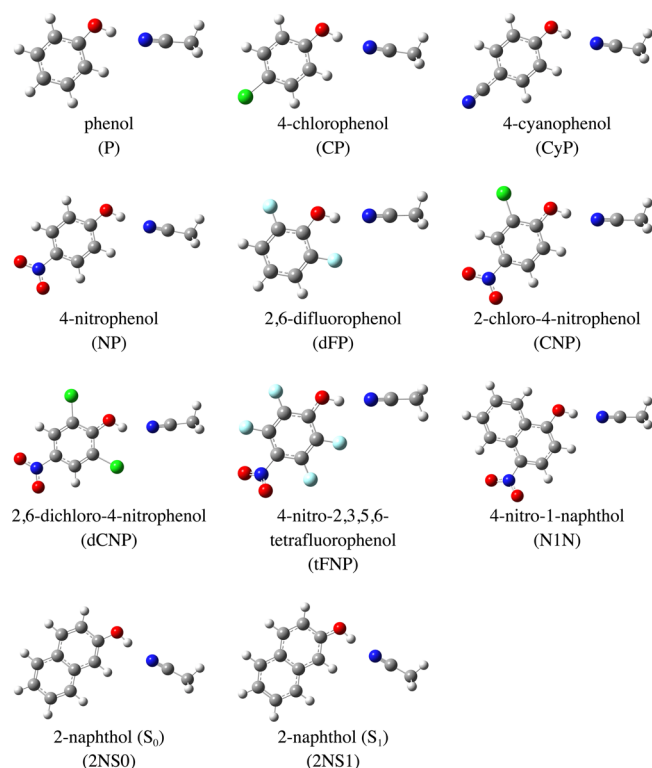


**Figure 1.** Test set of hydrogen bonded complexes of substituted phenols and naphthols with acetonitrile, depicted with gas phase optimized geometries: phenol (P), 4-chlorophenol (CP), 4-cyanophenol (CyP), 4-nitrophenol (NP), 2,6-difluorophenol (dFP), 2-chloro-4-nitrophenol (CNP), 2,6-dichloro-4-nitrophenol (dCNP), 4-nitro-2,3,5,6-tetrafluorophenol (tFNP), 4-nitro-1-naphthol (N1N), ground state 2-naphthol (2NS0), and the first excited state of 2-naphthol (2NS1). Alphanumeric codes corresponding to each complex are shown in parentheses.

Acetonitrile, with its relatively weak basicity, is a perfect match with the investigated acids, to cover the frequency range of O–H stretching transitions categorized as “weak hydrogen bonds”. Here, the observed O–H stretching frequency shifts are of such a strong magnitude that the local mode approach is maintained, as opposed to medium-strong hydrogen bonded systems where vibrational coupling with fingerprint and low-frequency modes complicate the vibrational mode description.<sup>40–48</sup> (b) Acetonitrile also enables a favorable 1:1 hydrogen bond complex formation with the aromatic alcohols in nonpolar solvents, which is difficult to achieve with protic hydrogen bond acceptor molecules like water or methanol, as these molecules have a tendency to self-complexation competing with the hydrogen bond complexation with the aromatic alcohols. (c) Acetonitrile does not contribute to the O–H stretching frequency region, avoiding spectral overlap issues. (d) Acetonitrile (being a small aprotic, polar, sterically unobtrusive molecule), has only limited internal degrees of freedom, making the small number of relevant geometries of hydrogen-bonded complexes an appealing feature. For a proper parametrization of the hydrogen bond in quantum chemical calculations, we compare our results on 2-naphthol with a collection of aromatic alcohols, all of which are hydrogen-bonded to acetonitrile and measured in the  $S_0$  state (Figure 1). These aromatic alcohols were chosen in such a way that the full range of O–H stretching frequency shifts is covered, including those of 2-naphthol in the  $S_0$  and  $S_1$  states. We analyze the solvent-dependent O–H stretching frequency shifts using TD-DFT calculations using a polarizable continuum model as implemented by Gaussian09. We further analyze these O–H stretching frequency shifts using the perturbative approach by Pullin.<sup>49–51</sup> We conclude that the slope of the observed O–H stretching frequency shifts as a function of solvent polarity is determined by solute–solvent couplings that are determined by the microscopic nature of a particular aromatic alcohol–acetonitrile complex. A clear trend is found between the O...N distance and the O–H stretching frequency at  $F_0 = 0$  ( $\epsilon_0 = 1$ ) from which we conclude that the O–H stretching frequency provides a direct measure of hydrogen bond distances of such aromatic alcohol complexes. On the basis of our findings, we show that the changes in hydrogen bond structure upon photoexcitation of 2-naphthol are significant, even though our analysis shows that the change in charge distribution when going from the  $S_0$  to the  $S_1$  state is minor. These structural changes can be correlated to the change in acidity, making the O–H stretching vibration not only a marker mode for the hydrogen bond geometry, but also for proton transfer reactivity.

## ■ DETAILS ON EXPERIMENTS AND CALCULATIONS

**Samples, Solvents, Steady-State and Time-Resolved Measurements.** The aromatic alcohols phenol (P), 4-chlorophenol (CP), 4-cyanophenol (CyP), 4-nitrophenol (NP), 2,6-difluorophenol (dFP), 2-chloro-4-nitrophenol (CNP), 2,6-dichloro-4-nitrophenol (dCNP), 4-nitro-1-naphthol (N1N), and 2-naphthol (2N) were purchased from Sigma-Aldrich and used as delivered. 2,3,5,6-tetrafluoro-4-nitrophenol (tFNP) was obtained by nitration of 2,3,5,6-tetrafluorophenol as detailed in the Supporting Information.  $pK_a$  values of these compounds are listed in Table 1. The solvents *n*-hexane, cyclohexane,  $CCl_4$ ,  $C_2Cl_4$ ,  $C_2HCl_3$ ,  $CHCl_3$ ,  $CH_2Cl_2$ , 1,2-dichloroethane, and acetonitrile (Sigma-Aldrich) were dried over molecular sieves. Care was taken that halogenated solvents contained only aprotic, if any, stabilizers. Steady-state FT-IR

**Table 1. Aqueous  $pK_a$  Values of the Aromatic Alcohols Used in This Study**

species	$pK_a$ value
P	9.95 <sup>a</sup>
2NS0	9.47 <sup>b</sup>
CP	9.38 <sup>a</sup>
CyP	7.95 <sup>a</sup>
NP	7.14 <sup>a</sup>
dFP	7.1 <sup>c</sup>
N1N	5.73 <sup>d</sup>
CNP	5.42 <sup>e</sup>
2NS1	3.00 <sup>b</sup>
dCNP	3.55 <sup>f</sup>
tFNP	2.81 <sup>g</sup>

<sup>a</sup>Reference 81. <sup>b</sup>Reference 81. <sup>c</sup>Reference 82. <sup>d</sup>Reference 83. <sup>e</sup>Reference 84. <sup>f</sup>Reference 85. <sup>g</sup>This work.

spectra were recorded with a Varian 640 FT-IR spectrometer. Ultrafast UV-pump mid-IR-probe measurements on 2-naphthol were performed as previously described.<sup>26,52–54</sup> Frequency positions of the O–H stretching bands have been obtained by applying Gaussian fits to the observed transitions contributing to the linear FT-IR or transient UV-pump-IR-probe spectra.

**Computational Methods.** All calculations were performed using density functional theory at the B3LYP level of theory<sup>55–58</sup> with the TZVP basis set<sup>59</sup> as implemented in Gaussian09.<sup>60</sup> The B3LYP functional was chosen for its ubiquitous utility in computational chemistry both in gas phase and solution phase modeling of chemical systems, and because it has been successfully applied to modeling solution phase vibrational frequencies.<sup>52,61</sup> (Additional preliminary calculations completed with the  $\omega$ B97XD functional are shown in the Supporting Information.) Excited state calculations were performed using the time-dependent density functional theory methods implemented in Gaussian09.<sup>62,63</sup> Each alcohol-acetonitrile complex was optimized in the gas phase. Harmonic vibrational frequencies with normal mode force constants, anharmonic vibrational frequencies with normal mode force constants, dipole moments, and dipole moment first derivatives were calculated for all gas phase optimized structures. Dipole moment second derivatives were obtained using

$$\mu'' = \frac{\partial(\mu')}{\partial x} = \frac{\mu'(x + \delta x) - \mu'(x - \delta x)}{2\delta x} \quad (1)$$

as the finite difference of dipole moment first derivatives with normal mode perturbations away from equilibrium by 1/1000 of the normalized amplitude.

Numerical Hessian calculations were required for computing the harmonic frequencies and force constants for the first excited state of the 2-naphthol complex. Direct calculation of anharmonic force constants for the 2NS1 complex could not be performed due to the absence of an analytically computed Hessian. Anharmonic force constants for 2NS1 were computed by finite difference of harmonic force constants obtained from calculations with near equilibrium perturbations along the O–H stretching normal mode.

Solution phase calculations were carried out using a polarizable continuum model according to the integral equation formalism (IEF-PCM)<sup>64–67</sup> with atomic radii cavity definitions according to the Universal Force Field (UFF) model as implemented in Gaussian09.<sup>60</sup> Results from solution phase

calculations were obtained from complexes that were geometry optimized in the PCM reaction field. PCM models mitigate the computational burden of explicitly modeling solvent molecules and the specific interactions with the solute. The solvent is treated as a constant dielectric reaction field where the charge density of the solute is projected onto a grid on the surface of a solvent cavity and polarized based on the value of the solvent dielectric. The resulting polarized charges on the cavity affect the charge density of the molecule and so on until self-consistency is achieved. Additional terms for cavitation, dispersion, and other specific interactions may be included for more accuracy. A critical assumption for implicit solvation models is that the interactions between solute and solvent can be uniformly modeled by a constant dielectric where specific solute–solvent interactions can be neglected. Preliminary solution phase results suggested that solution phase calculations using implicit solvation were in systematic error due to an overstabilization occurring while using default atomic radii definitions. Since there is not yet a proper protocol for scaling harmonic frequencies calculated in implicit solvation, we fit a scaling factor adjusting the default UFF atomic radii by 1.35 to obtain a better agreement with measured slopes. Similar scaling factors have been implemented in previous studies using implicit solvation to model aromatic systems in nonpolar, low-dielectric solvents.<sup>68–70</sup> Atomic charges were computed in both gas and solution phase using Mulliken Population Analysis.<sup>71</sup>

For consistency with experimental measurements, gas phase vibrational frequencies were extrapolated from the plot showing the change in the harmonic vibrational frequencies versus the solvent dielectric function,  $F_0$ . Because of harmonic approximations used in the calculation of vibrational frequencies, scaling factors for the extrapolated gas phase frequencies were necessary for proper quantitative comparison to experimental values. A gas phase scaling factor of 0.956 was obtained by minimizing the error between computed and experimentally determined gas phase vibrational frequencies. As an additional comparison, direct computations of gas phase vibrational frequencies yielded a scaling factor of 0.958, which is in excellent agreement with the extrapolated scaling factor. Scaling factors show reasonable agreement compared to experimentally measured gas phase frequencies with a mean absolute deviation of 17.9  $\text{cm}^{-1}$  and are consistent with typical scaling factors used for larger test sets.<sup>72–74</sup> Additional gas phase calculations were performed to provide support for using the uniform scaling factor for the 2NS1 species. Measured gas phase O–H stretching frequency data is available for 2-naphthol, 2-naphthol– $\text{H}_2\text{O}$ , 2-naphthol– $\text{CH}_3\text{OH}$ , 2-naphthol– $\text{NH}_3$ , and 2-naphthol– $\text{NH}_2\text{CH}_3$ .<sup>33,34,37</sup> The predicted scaling factors for gas phase complexes with similar O–H stretching frequencies 2-naphthol (3609  $\text{cm}^{-1}$ ), 2-naphthol– $\text{H}_2\text{O}$  (3408  $\text{cm}^{-1}$ ), and 2-naphthol– $\text{CH}_3\text{OH}$  (3303  $\text{cm}^{-1}$ ) are 0.955, 0.978, and 0.973, respectively. The additional gas phase calculations are presented in a correlation plot with measured values in the Supporting Information, Figure S2. The predicted scaling factor for 2NS1 (3361  $\text{cm}^{-1}$ ) is 0.962. These scaling factors are in reasonable agreement with the uniform scaling factor 0.958.

Final computed properties for N1N, CNP, 2NS0, and 2NS1 contained averaging to account for separate rotational conformations where rotation around the C–OH bond was not symmetrical. Calculated parameters for these complexes were obtained by taking a Boltzmann weighted average of the two rotamers based on the relative energies of the optimized gas phase complexes.

## EXPERIMENTAL RESULTS

Figure 2 summarizes our experimental results obtained on the O–H stretching region of mixtures of the aromatic alcohols

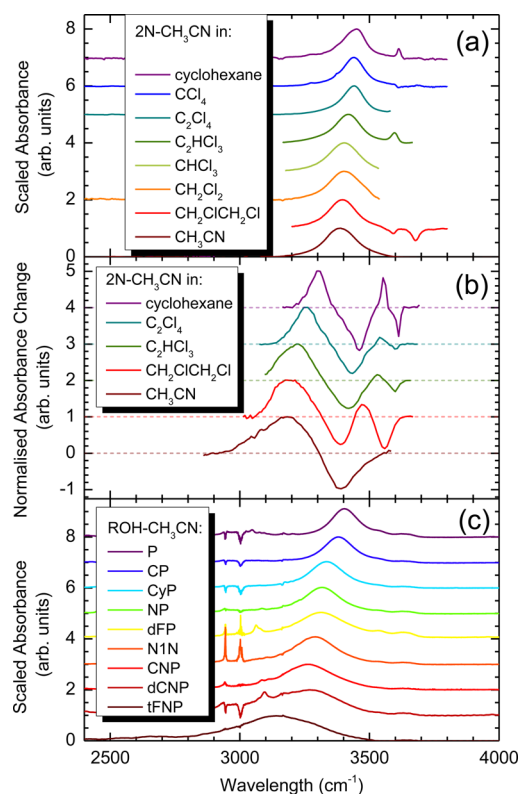


**Figure 2.** (a) Steady-state IR spectra and (b) transient IR spectra at 20 ps after UV excitation of the 2-naphthol-acetonitrile complex in dissolved in media of various dielectric constants. Steady-state FT-IR spectra (c) of selected substituted phenols and 1-naphthol hydrogen-bonded complexes in acetonitrile solution.

and acetonitrile in solvents of different polarity. Typically, one can distinguish between the narrow O–H stretching band of uncomplexed chromophores around  $3600\text{ cm}^{-1}$  and the much broader red-shifted O–H stretching bands of chromophores hydrogen-bonded to acetonitrile. The position of the O–H stretching band of these hydrogen-bonded complexes depends on the nature of the aromatic alcohol as well as on the polarity of the solvent. To further illustrate the impact of these effects having different molecular origin, we have added additional panels of steady-state FT-IR spectra in the Supporting Information (Figure S1). In Figure 2a, the FT-IR spectra are shown for 2N–CH<sub>3</sub>CN in the  $S_0$  state as measured in solvents of different polarity. The observed O–H stretching band does not change much in frequency position and spectral width. Figure 2b shows the transient UV-pump-IR-probe spectra measured at a pulse delay of 20 ps for 2N–CH<sub>3</sub>CN in solvents of different polarity. Negative signals indicate bleach contributions of 2N–CH<sub>3</sub>CN in the  $S_0$  state. Positive signals appearing at clearly red-shifted frequency positions show where 2N–CH<sub>3</sub>CN has its O–H stretching band in the  $S_1$  state. The data shown in Figure 2 have been recorded at large pulse delay, when the hydrogen-bonded complex has reached a state where reorganization dynamics induced by the optical excitation is completed. The observed frequency shifts are similar after electronic excitation and completion of solvation dynamics.

This result supports the notion<sup>52,53</sup> that, upon electronic excitation from the  $S_0$  to the  $S_1$  state, the observed O–H stretching frequency shifts are predominantly due to electronic charge redistribution within the hydrogen-bonded complex. Figure 2c shows that the set of aromatic alcohols chosen for this study covers a larger spectral range for the O–H stretching band. In particular, the observed O–H stretching band for 2N–CH<sub>3</sub>CN in the  $S_0$ - and the  $S_1$  states falls within this spectral range making it possible to test the assumption that the O–H stretching mode is a local probe for the hydrogen bond strength, correlating the O–H stretching mode with acidity ( $pK_a$  values).

From our results, the following features can be given: (a) the larger the acidity (and concomitantly the lower the  $pK_a$  value), the larger the observed down-shift of the O–H stretching band and the larger the associated spectral width for a given solvent with a particular dielectric constant; (b) the O–H stretching frequency red-shift and spectral width increases with increasing solvent polarity for a given aromatic alcohol hydrogen-bonded to acetonitrile; (c) the observed O–H stretching frequency red-shifts, as a function of solvent polarity, are larger for the 2-naphthol-acetonitrile complex than for the previously reported values of uncomplexed 2-naphthol;<sup>52</sup> (d) the O–H stretching frequency red-shift and spectral width are larger for 2N–CH<sub>3</sub>CN in the  $S_1$  than in the  $S_0$  state; (e) the O–H stretching band of the hydrogen-bonded complexes of the aromatic alcohols with acetonitrile studied has typically a (nearly) symmetrical line shape without substructure, supporting the ansatz that the O–H stretching vibration is a local mode not significantly altered in nature by couplings with other vibrational degrees of freedom, including the Fermi resonance with the O–H bending overtone; (f) the O–H stretching transitions of 2N–CH<sub>3</sub>CN in the  $S_0$  and  $S_1$  states are located within the spectral range covered with the set of aromatic alcohols in this study.

We find that the frequency shifts exhibit a linear dependence as a function of the solvent polarity function:

$$F_0 = \frac{2\varepsilon_0 - 2}{2\varepsilon_0 + 1} \quad (2)$$

where  $\varepsilon_0$  is the static dielectric constant of the solvent (Figure 3a). From this we can conclude that the solute–solvent interaction results in a solvent-dependent O–H stretching frequency of the hydrogen-bonded complexes, with the intercept at  $F_0 = 0$  ( $\varepsilon_0 = 1$ ) representing the gas phase medium-free case and a slope reflecting the impact on the local O–H stretching mode by the coupling of the molecular complex to the dielectric medium. The intercept appears to follow the trend in  $pK_a$  values; i.e., a lower  $pK_a$  value bears a more red-shifted intercept. For most of the investigated molecular systems, the slope follows a similar trend with lower  $pK_a$  values yielding larger slopes. However, the slopes for the 2,6-disubstituted aromatic alcohols, i.e., dFP and dCNP, have smaller values than what the overall trend suggests. In addition, the slope for 2NS1 is clearly larger.

A closer inspection of the obtained O–H stretching intercept and slope values of the investigated phenol and naphthol complexes results in the important finding that the intercept value correlates strongly with the acidity of the aromatic alcohols. By plotting the values for the intercept as a function of the  $pK_a$  value in Figure 4, we demonstrate that the intrinsic O–H stretching frequency of the molecular complexes can be

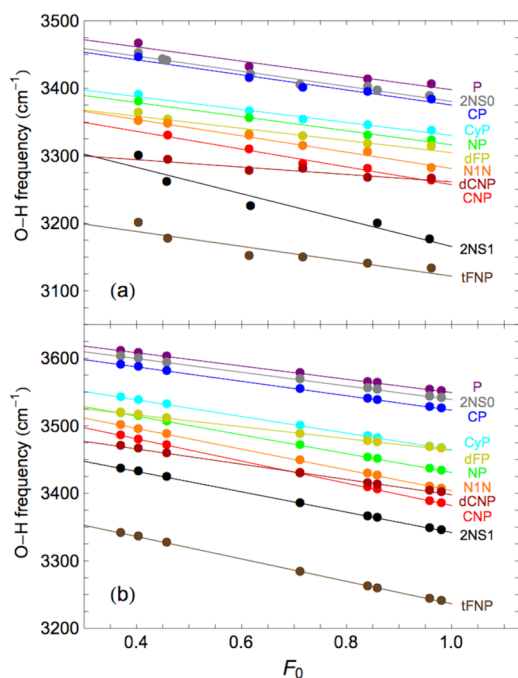


**Figure 3.** Plot of (a) the experimentally measured and (b) calculated B3LYP O–H stretching frequency versus solvent dielectric function ( $F_0$ ). Line fits are shown color-coded for each set of experimentally measured points corresponding to a given aromatic alcohol–acetonitrile complex. Calculated line fits were obtained by using PCM model slope values.

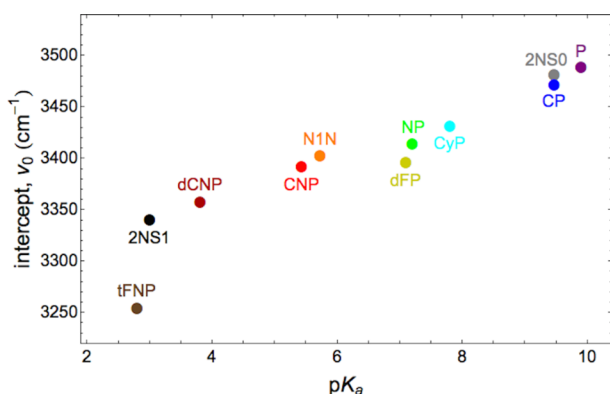


**Figure 4.** Correlation between the experimentally derived O–H stretching frequency for the gas-phase medium-free hydrogen-bonded complexes ( $F_0 = 0$ ) and the  $pK_a$  values reported for the aromatic alcohols.

considered as a marker mode for the proton chemical reactivity of the aromatic alcohols. Hence, a direct connection between O–H stretching frequencies of the gas-phase medium-free hydrogen bonded complexes and hydrogen bond structure must exist, because hydrogen bond structure is regarded to be directly governing acid–base chemical reactivity.

## COMPUTATIONAL RESULTS

**PCM Model.** PCM models mitigate the computational burden of explicitly modeling solvent molecules and the specific interactions with the solute. The solvent is treated as a constant dielectric reaction field where the charge density of the solute is projected onto a grid on the surface of a solvent cavity and polarized based on the value of the solvent dielectric. The

resulting polarized charges on the cavity affect the charge density of the molecule and so on until self-consistency is achieved. Additional terms for cavitation, dispersion, and other specific interactions may be included for more accuracy. A critical assumption for implicit solvation models is that the interactions between solute and solvent can be uniformly modeled by a constant dielectric where specific solute–solvent interactions can be neglected.

**Pullin Model.** To model the impact of solute–solvent interactions on vibrational marker modes we have previously applied a perturbative treatment.<sup>52,53</sup> This approach has the gas phase vibrational Hamiltonian amended with the Onsager expression for solute–solvent interactions assuming a dielectric continuum for the solvent, as derived by Pullin,<sup>50,51</sup> and has the time-dependent solvent response to electronic excitation implemented using the van der Zwan–Hynes relationship.<sup>75–77</sup>

Assuming that the solvation shell reorganization has been completed at long times, an analytical equation for the solvent-induced vibrational frequency shift,  $\Delta v_i$ , of normal mode  $i$  can be given, as follows:<sup>53</sup>

$$\Delta v_i = \frac{v_0^i F_0}{2V_i'' \alpha_i^3} \left( \mu_i'' \mu_i^0 - \frac{V_i'''}{V_i''} \mu_i' \mu_i^0 \right) + \frac{v_0^i F_\infty}{2V_i'' \alpha_i^3} (\mu_i'' \mu_i^0 + \mu_i' \mu_i') \quad (3)$$

describing the change in vibrational frequency as a function of the solvent dielectric constant, gas phase dipole and force constant parameters. Here, the solute parameters are the gas phase vibrational frequency ( $v_0^i$ ), quadratic force constant ( $V_i''$ ), cubic force constant ( $V_i'''$ ), dipole moment ( $\mu_i^0$ ), dipole moment first derivative ( $\mu_i'$ ), and dipole moment second derivative ( $\mu_i''$ ). The solute–solvent interactions are taken into account with the solvent parameters: static dielectric constant function ( $F_0$ ) and the optical dielectric constant function ( $F_\infty$ ) as well as the solute cavity volume ( $\alpha_i^3$ ). In this study, the solute cavity volume  $\alpha_i^3$  is calculated from the Kirkwood–Onsager equation:

$$E_{sol} = -\frac{\mu^2 F_0}{2\alpha^3} \quad (4)$$

where  $\epsilon_0$  is the static dielectric constant of the solvent,  $F_0$  is the solvent dielectric function from eq 2 and  $F_\infty$  is

$$F_\infty = \frac{2\epsilon_\infty - 2}{2\epsilon_\infty + 1} \quad (5)$$

with  $\epsilon_\infty$  representing the dielectric constant of the solvent at optical frequencies.

In a comparison of solution phase vibrational frequencies versus solvent dielectric function,  $F_0$ , the key terms of eq 3 are the slope  $S_i$

$$S_i = \frac{v_0^i}{2V_i'' \alpha_i^3} \left( \mu_i'' \mu_i^0 - \frac{V_i'''}{V_i''} \mu_i' \mu_i^0 \right) \quad (6)$$

and intercept  $B_i$

$$B_i = \frac{v_0^i F_\infty}{2V_i'' \alpha_i^3} (\mu_i'' \mu_i^0 + \mu_i' \mu_i') \quad (7)$$

respectively. The slope,  $S_i$ , represents a direct relationship describing how the solvent affects the vibrational frequency of a given normal mode,  $i$ . The intercept,  $B_i$ , is dominated by molecular parameters of the vibrational mode that, apart from a scaling factor, reflects the intrinsic properties of the chemical bond for which normal mode  $i$  is a local probe. The values of

the intercepts will strongly depend on the particular properties of the molecular complex. For instance, the vector dipole moment can vary substantially upon substitution at the ortho, meta, and para positions of the aromatic alcohols.

**Comparing the Outcome of the PCM and of Pullin Models.** Figure 3b shows the O–H stretching frequency for the aromatic alcohol–acetonitrile complexes as a function of  $F_0$ , calculated using the PCM model. Trends are observed similar to those noted for the experimental results. Indeed a direct correlation between  $pK_a$  value and O–H stretching frequency, as well as between the  $pK_a$  value and intercept and slope, is apparent. Closer inspection shows, again, that the ortho-substituted aromatic alcohols have a different trend in the value for the slope than the unsubstituted complexes. In addition, the calculated slope value for 2NS1 is clearly smaller for the calculated case than that obtained from experiment.

We obtained the values for the intercept and slope for solvent-induced vibrational frequency shifts of the aromatic alcohol–acetonitrile complexes in a different way for the two methods. For the PCM model, intercept and slope values were obtained by fitting lines to the explicitly calculated O–H stretching vibrational mode frequencies versus  $F_0$  of solution phase optimized complexes. For the Pullin model, we can directly calculate the parameters as defined in eqs 5 and 6. We have summarized our results in Table 2.

The differences between the two methodologies are subtle as both the PCM and Pullin models use implicit solvation models to arrive at the solvent induced vibrational frequency shifts. However, the Pullin model is based on the Kirkwood–Onsager

**Table 2. O–H Stretching Frequency Slope Values for Aromatic Alcohol–CH<sub>3</sub>CN Complexes from Experiment and Calculations Using the PCM and the Pullin Models**

species	experiment (cm <sup>-1</sup> )	PCM (cm <sup>-1</sup> )	PCM-Δ <sup>a</sup> (cm <sup>-1</sup> )	PCM-B <sup>b</sup> (cm <sup>-1</sup> )
P	105.9	98.2	-7.5	3487.8
2NS0	111.9	99.2	-10.7	3480.6
CP	111.7	106.8	-4.8	3471.0
CyP	95.9	123.1	+27.3	3430.6
NP	104.4	139.5	+34.7	3413.7
dFP	90.1	89.5	-2.2	3395.7
N1N	121.0	152.1	+32.5	3401.7
CNP	131.7	163.6	+33.0	3391.2
2NS1	195.3	190.8	-44.8	3339.6
dCNP	54.7	116.6	+58.4	3357.2
tFNP	110.2	168.2	+55.9	3253.4

species	gas phase (cm <sup>-1</sup> )	Pullin (cm <sup>-1</sup> )	Pullin-Δ <sup>a</sup> (cm <sup>-1</sup> )	Pullin-B <sup>b</sup> (cm <sup>-1</sup> )
P	3487.4	102.6	-3.4	9.8
2NS0	3477.0	113.7	+7.2	11.6
CP	3470.8	92.0	-19.7	8.4
CyP	3430.9	104.2	+8.2	8.9
NP	3413.4	104.0	-0.5	8.9
dFP	3400.2	132.0	+41.9	14.0
N1N	3399.4	115.3	-5.8	10.1
CNP	3386.0	107.2	-24.6	8.9
2NS1	3341.3	188.6	-43.1	12.0
dCNP	3361.7	88.3	+33.5	6.7
tFNP	3257.9	131.8	+21.5	11.4

<sup>a</sup>Δ is the theory slope value minus experimental slope value. <sup>b</sup>B is the slope intercept value.

equation (eq 3), where the solvation energy is calculated as the difference between the electronic energy of the implicit solution phase optimized structure. The calculated slope depends heavily upon the gas phase dipole moment since the molecular dipole moment and its derivatives vary consistently as a function of the dielectric constant. The PCM model relies heavily on the accuracy of the electronic energy in the PCM reaction field. Here, the vibrational frequencies depend upon the accuracy of the second derivative of the energy with respect to the nuclear positions. The accuracy of the modeled electronic energy and nuclear positions in the reaction field are critical for correct modeling of the solution phase vibrational energies, and thus, the solvent induced vibrational frequency shifts. Both models neglect specific solute–solvent interactions, which is where the vast majority of the error in each model is presumed to originate. Computationally, both models require PCM optimizations with frequency analysis (to confirm a minimum structure); however, the Pullin model also requires a gas phase optimization in addition to an anharmonic frequency analysis, which is a costly additional time burden by comparison.

To have a closer look at the outcome of the calculations using these two methods, we have plotted in Figure 5 the resulting dependencies of the calculated slope and intercept as black dots and compare these with the experimentally determined values (red dots). The dCNP and 2NS1 complex are clear outliers within the set of measured data. For the dCNP complex, the steric hindrance of the ortho-substituted chlorine groups may be a factor in the low slope value. Similar low slope values are also seen for the tFNP and dFP complexes, which may hint at similar underlying geometric reasons. Instead, the 2NS1 complex has a higher slope than the other substituted complexes suggesting a larger effect of solute–solvent coupling than for the other complexes.

In an effort to clarify the obtained data and establish possible relationships between intercept and slope, a line fit is drawn through the slope values as a function of intercept of the single substituted aromatic alcohol complexes using a least-squares fitting. From the measured slope values, the single substituted complexes do not appear to have a clear trend related to slope values versus the intercept, thus showing that only a weak correlation exists between these two quantities for this set of molecular systems. From the calculated data using the PCM model (Figure 5a), the line fit to single substituted species suggests a trend for the para-substituted phenol–CH<sub>3</sub>CN complexes. Despite this clear trend, the line fit significantly deviates from the experiment. Multiple substituted complexes show an increasing deviation of the slope value for a smaller intercept. Such a trend is not suggested when the Pullin model is used (Figure 5b). The slope value for 2NS1 slope remains underestimated with the Pullin model compared to experiment, but is in agreement with the resulting slope value using the PCM model. The tFNP, dCNP, and dFP complexes have computed slopes that are overestimations in the range of 21.5–41.9 cm<sup>-1</sup> compared to experiment. Nevertheless, slope values calculated with the Pullin model are in better agreement with experiment compared to those obtained with the PCM model, having mean absolute deviations of 25.6 and 20.9 cm<sup>-1</sup> for PCM and Pullin, respectively. We thus conclude that the Pullin model represents a better description of solvent-induced vibrational frequency shifts for O–H stretching modes of aromatic alcohols hydrogen-bonded to acetonitrile.

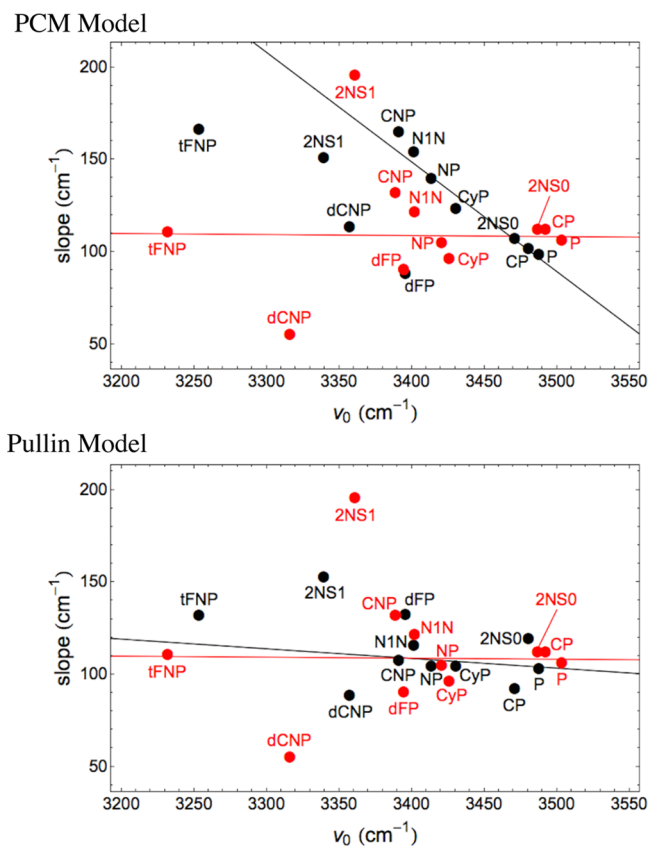


**Figure 5.** O–H stretching vibrational frequency slope versus intercept plots for alcohol-acetonitrile complexes in low dielectric solvents versus extrapolated gas phase vibrational frequencies. Experimentally measured data points and line fits are shown in red while calculated slopes for are shown in black. (a) PCM model slopes are fit to explicitly computed frequencies in implicit solvent. (b) Pullin model slopes are calculated by the perturbative treatment of gas and solution phase properties using eq 4. Line fits to calculated and measured slopes only include the single substituted complexes whereas multiple substituted complexes tFNP, dCNP, 2NS1, CNP, and dFP species have been left out for the line fits.

## DISCUSSION ON ACID–BASE HYDROGEN BOND STRUCTURE

On the basis of the comparison between experiments and calculations in Figures 3 and 5, as well as Table 2, we can argue that the Pullin model leads to a better description of the structure of the hydrogen bonded aromatic alcohol-acetonitrile complexes. We can now analyze the structural properties as predicted by the Pullin model. Here, we aim to obtain correlations between our observables, the intercept and slope of the solvent-dependent O–H stretching frequencies of the complexes, and structural parameters providing insight into electronic and nuclear degrees of freedom, i.e., internuclear distances and electronic charge densities.

Tables 3 and 4 summarize our findings on the distances between the oxygen on the parent alcohol and the nitrogen in acetonitrile (O $\cdots$ N) and alcohol O–H distances in the hydrogen-bonded complexes, respectively. By plotting the results on the O $\cdots$ N distance in Figure 6 (and those obtained on the O–H distance in the Supporting Information, Figure S3), we learn that the value for the intercept is strongly correlated with the O $\cdots$ N and O–H distances of the complexes, whereas the slope value is not directly correlated to the

**Table 3.** Calculated O $\cdots$ N Bond Distances in the Gas Phase and Various Low Dielectric Solvents<sup>a</sup>

complex <sup>b</sup>	gas	sol. A $\epsilon = 1.88$	sol. B $\epsilon = 2.02$	sol. C $\epsilon = 2.27$
P	2.962	2.933	2.930	2.926
2NS0	2.953	2.924	2.923	2.918
CP	2.944	2.914	2.911	2.907
CyP	2.913	2.883	2.880	2.876
NP	2.901	2.869	2.866	2.862
dFP	2.876	2.854	2.852	2.849
N1N	2.890	2.857	2.855	2.851
CNP	2.872	2.843	2.841	2.837
2NS1	2.868	2.837	2.835	2.831
dCNP	2.842	2.817	2.815	2.811
tFNP	2.798	2.771	2.769	2.765
complex <sup>b</sup>	sol. D $\epsilon = 4.71$	sol. E $\epsilon = 8.93$	sol. F $\epsilon = 10.13$	sol. G $\epsilon = 35.69$
P	2.908	2.899	2.898	2.891
2NS0	2.900	2.891	2.890	2.883
CP	2.889	2.880	2.879	2.872
CyP	2.858	2.849	2.848	2.842
NP	2.843	2.834	2.833	2.826
dFP	2.837	2.831	2.831	2.827
N1N	2.831	2.821	2.820	2.813
CNP	2.820	2.812	2.811	2.805
2NS1	2.813	2.805	2.804	2.798
dCNP	2.798	2.792	2.791	2.787
tFNP	2.750	2.743	2.742	2.737

<sup>a</sup>Modeled solvents are as follows: (a) *n*-hexane, (b) cyclohexane, (c) tetrachloroethane, (d) chloroform, (e) dichloromethane, (f) dichloroethane, (g) acetonitrile. <sup>b</sup>Complexes are presented in order of ascending calculated gas phase vibrational frequency.

internuclear distances describing the hydrogen bond geometries. It follows that the more red-shifted the O–H stretching frequency, the shorter the O $\cdots$ N and concomitantly the larger the O–H distances are for the gas phase complexes. From this, we conclude that within the set of aromatic alcohol-acetonitrile complexes studied, the intercept value can be directly interpreted as a structural indicator. Whereas, solute-solvent couplings and geometric properties, which are specific for each complex, strongly determine the outcome of the slope.

An examination of the bond lengths in Tables 3 and 4 gives clear and consistent trends for shorter (O $\cdots$ N) distances as the solvent dielectric is increased and as the frequency of the O–H stretching oscillator decreases due to substituent effects. These trends are complemented by a consistent relationship for longer O–H bond lengths as the solvent dielectric is increased and as the energy of the O–H stretching oscillator decreases due to substituent effects. This is an expected result indicating that the surrounding solvent stabilizes the complex with stronger hydrogen bonds and slightly weaker O–H bonds as the solvent dielectric is increased. Bond length trends for O $\cdots$ N and O–H bond distances versus gas phase O–H stretching frequency are consistent among the set as the dielectric of the solvent is increased with the exception of the O $\cdots$ N bond length of dFP in lowest dielectric solvents and a very slight deviation in the O–H bond length of 2NS1 in the highest dielectric solvents.

Table 5 lists the calculated values for the gas phase Mulliken atomic charges (obtained from a partitioning of the charge density based on the electronic overlap integrals)<sup>71</sup> of specific atomic species or moieties for each complex. Oxygen and

**Table 4. Calculated O–H Bond Distances in the Gas Phase and Various Low Dielectric Solvents<sup>a</sup>**

complex <sup>b</sup>	gas	sol. A $\epsilon = 1.88$	sol. B $\epsilon = 2.02$	sol. C $\epsilon = 2.27$
P	0.973	0.974	0.974	0.975
2NS0	0.973	0.975	0.975	0.975
CP	0.973	0.975	0.975	0.976
CyP	0.975	0.978	0.978	0.978
NP	0.977	0.979	0.979	0.980
dFP	0.978	0.980	0.980	0.980
N1N	0.977	0.980	0.980	0.981
CNP	0.979	0.981	0.981	0.982
2NS1	0.981	0.984	0.984	0.984
dCNP	0.981	0.983	0.983	0.983
tFNP	0.987	0.989	0.989	0.989
complex <sup>b</sup>	sol. D $\epsilon = 4.71$	sol. E $\epsilon = 8.93$	sol. F $\epsilon = 10.13$	sol. G $\epsilon = 35.69$
P	0.976	0.976	0.976	0.977
2NS0	0.976	0.977	0.977	0.978
CP	0.977	0.978	0.978	0.978
CyP	0.980	0.981	0.981	0.981
NP	0.981	0.982	0.982	0.983
dFP	0.981	0.981	0.981	0.982
N1N	0.982	0.983	0.984	0.984
CNP	0.983	0.984	0.984	0.985
2NS1	0.986	0.987	0.987	0.988
dCNP	0.984	0.985	0.985	0.986
tFNP	0.991	0.991	0.991	0.993

<sup>a</sup>Modeled solvents are as follows: (a) *n*-hexane, (b) cyclohexane, (c) tetrachloroethene, (d) chloroform, (e) dichloromethane, (f) dichloroethane, and (g) acetonitrile. <sup>b</sup>Complexes are presented in order of ascending calculated gas phase vibrational frequency.

hydrogen charges appear to follow a general trend of charge transfer away from the oxygen and hydrogen centers as the gas phase O–H stretching frequency is decreased. Figure 7 shows the relationship between computed oxygen charge and O...N distance. Relatively small amounts of charge are distributed away from the acetonitrile moiety for all complexes. Carbon centers bonded to substituent fluorine atoms in the dFP and tFNP complexes show charge transfer away from the carbon atoms toward the fluorine atoms due to differences in electronegativity. The oxygen center in the dFP species appears to be susceptible to charge density loss due to the increase in the solvent dielectric.

We are now in the position to address the questions on hydrogen bond structure for the electronically excited state of 2-naphthol. The direct comparison with the other aromatic alcohol-acetonitrile complexes shows that 2NS1 fully behaves like the other hydrogen-bonded complexes in this set. As such, we can conclude that (a) the hydrogen bond between 2-naphthol and acetonitrile becomes stronger upon excitation to the S<sub>1</sub> state and (b) the associated charge distribution changes on the oxygen and hydrogen atom within the hydrogen bond are minimal. On the basis of our joint experimental and theoretical approach we derive an O...N distance change from 2.953 to 2.868 Å caused by optical excitation of 2N–CH<sub>3</sub>CN in the gas phase, i.e., a decrease of 2.9% that can be compared to distance changes in 2NS0 imposed by the solvent of less than 2.4% for the most polar solvents in this study. For the calculated O–H distance, we derive a change from 0.973 to 0.981 Å caused by optical excitation, i.e. an increase of 0.8%. Such a change is only slightly larger than the 0.5% increase

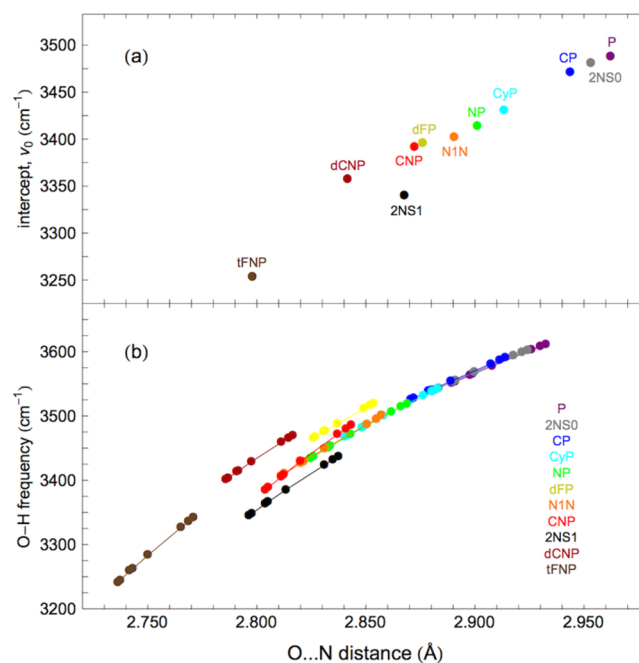


**Figure 6.** Calculated O–H stretching frequency versus O...N distance for the hydrogen-bonded complex. The upper panel (a) shows the calculated intercept value representing the O–H stretching frequency for the gas phase case (with frequency scaling adjusted to reported experimental values of gas phase 2-naphthol clusters); the lower panel (b) shows the nonscaled frequency spread for eight different solvent dielectric models, representing the different solvents studied. (Each complex is indicated with a specific color. Highest frequencies correspond to solvent dielectric of  $\epsilon = 1.9$  and lowest frequencies correspond to solvent dielectric of  $\epsilon = 78.4$ .)

found for the O–H distance when comparing the 2NS0 complex in the gas phase and in acetonitrile.

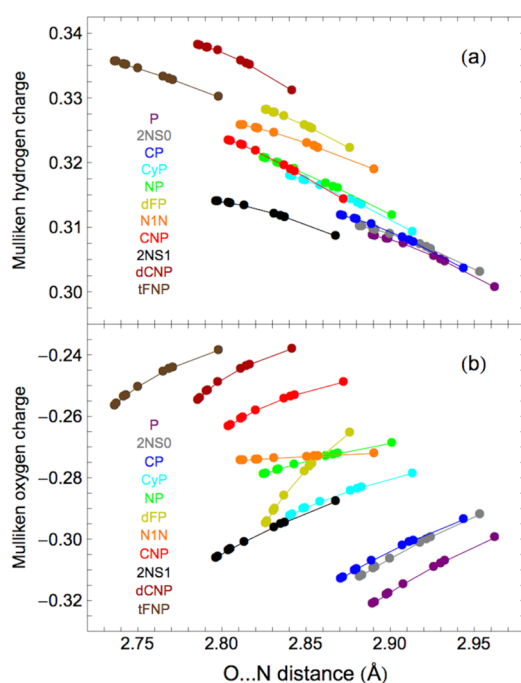
The calculated Mulliken charges on the oxygen and hydrogen atoms as a function of the hydrogen bond O...N distance are shown in Figure 7, calculated for the different dielectric continuum solvents as well as for the gas phase. Clear trends are present in these data: the larger the acidity (the lower the  $pK_a$ ), the less negative partial charge is present on the oxygen atom and the more positive partial charge can be found on the hydrogen atom. This is in line with the general understanding of the electronegative substituents causing a net charge flow from the O–H group to the aromatic ring. This effect of net partial charge flow, upon examining the series of aromatic alcohol-acetonitrile complexes, appears to show a consistent change with acidity strength. These changes are larger than the overall range of charge flow on the oxygen and hydrogen atoms caused by the dielectric medium, though the impact of the solvent is dependent on the specific aromatic alcohol, which may have its origin in the specific geometric details for each complex. In a comparison of the values obtained for 2NS0 and 2NS1, we conclude that the impact of the electronic excitation on the net charge flow from the hydrogen bond is minimal. For the oxygen atom, the charge changes from  $-0.292$  (2NS0) to  $-0.288$  (2NS1), which is a 1.4% decrease of negative charge. For the hydrogen atom, we calculate that the Mulliken charge changes from  $+0.303$  (2NS0) to  $+0.308$  (2NS1), which is an increase of 1.7% in positive charge.

Figure 8 shows the correlation between hydrogen bond distances and atomic charges with  $pK_a$ 's of aromatic alcohols in

Table 5. Calculated Mulliken Gas Phase Atomic Charges for Atoms and Atomic Moieties of Aromatic Alcohol Complexes

complex <sup>a</sup>	O	H	ACN <sup>b</sup>	$\alpha$ -C	<i>o</i> -C	<i>m</i> -C	<i>p</i> -C	other <sup>c</sup>
P	-0.299	+0.300	+0.024	+0.095	-0.341	-0.193	-0.134	+0.549
2NS0	-0.292	+0.303	+0.025	+0.113	-0.371	-0.029	+0.041	+0.209
CP	-0.294	+0.303	+0.026	+0.094	-0.326	-0.071	-0.124	+0.392
CyP	-0.279	+0.309	+0.030	+0.105	-0.317	-0.174	-0.042	+0.368
NP	-0.269	+0.311	+0.031	+0.105	-0.292	-0.251	-0.022	+0.386
dFP	-0.265	+0.321	+0.025	-0.106	+0.470	-0.352	-0.073	-0.020
N1N	-0.272	+0.318	+0.031	+0.083	-0.220	-0.152	+0.029	+0.183
CNP	-0.249	+0.313	+0.033	+0.184	-0.300	-0.202	-0.005	+0.225
2NS1	-0.288	+0.308	+0.030	+0.117	-0.358	-0.071	+0.043	+0.219
dCNP	-0.238	+0.329	+0.024	+0.330	-0.436	-0.098	-0.001	+0.089
tFNP	-0.238	+0.328	+0.039	-0.027	+0.326	+0.491	-0.197	-0.722

<sup>a</sup>Complexes are listed in ascending order according to calculated gas phase O–H stretching frequency. <sup>b</sup>Sum of charges for atomic centers in the acetonitrile moiety. <sup>c</sup> $\alpha$ -C is the carbon atom bonded to the alcohol oxygen; *o*-C are the carbon atoms *ortho* to the alcohol group; *m*-C are the carbon atoms *meta* to the alcohol group; *p*-C is the carbon atom *para* to the alcohol group. Sum of charges are for all other atomic centers in the complex.



**Figure 7.** Calculated Mulliken charges on the oxygen (a) and hydrogen atom (b) versus O...N distance for each complex for eight different dielectric constants representing different solvents used in this study. The ninth point representing the largest O...N distance value refers to the gas phase case. (Points corresponding to particular complexes are distinguished by color.)

1:1 complexes with ACN. It follows that a clear trend is present for the O...N and O–H distances (Figure 8a,b), the larger the acidity (the smaller the  $pK_a$  value), the smaller the O...N distances (the larger the O–H distances). Similar trends are found for the Mulliken charges of the oxygen and hydrogen atoms within the hydrogen bond as well as for the sums of the Mulliken charges of the acetonitrile molecule and of the remaining part of the aromatic system (Figures 8c–f). While the value for 2NS1 falls clearly within the observed trends for the O...N and O–H distances, somewhat larger deviations occur for the correlation diagrams of the Mulliken charges. One should note, however, that the Mulliken charges in 2NS1 do not deviate too much. Instead our results confirm the previously reported findings of an only minimal change in electronic charge distribution upon excitation of the  $S_0 \rightarrow {}^1L_b$

transition in 2-naphthol. As has been stated before in the literature, photoinduced charge distribution changes are expected to be more pronounced in the conjugate photobase than in the photoacid form, making the driving force for photoacidity to lie heavily on the conjugate photobase side of the Förster cycle.<sup>30,31,39</sup> Despite these minor changes in electronic charge distributions upon electronic excitation in the photoacid form of 2-naphthol, the hydrogen bond geometry of the 2N–CH<sub>3</sub>CN complex does change within the parameter range correlating with the well-known change in acidity.

## CONCLUSIONS

We have investigated the transient response of the local O–H stretching mode of the 2N–CH<sub>3</sub>CN hydrogen bonded complex by combining femtosecond pump–probe UV-IR spectroscopy and a theoretical treatment of solvatochromic effects based on the Pullin perturbative approach parametrized at the DFT level. We focused on the effect of solute–solvent couplings on the observed O–H stretching of complexes in the  $S_0$  electronic ground state as compared to 2N in the  ${}^1L_b$  electronic excited state in solvents of different polarity. We have also compared the OH vibration in the 2N–CH<sub>3</sub>CN complex to the corresponding mode in a collection of aromatic alcohol–acetonitrile complexes using substituted phenols and naphthols covering the 3000–3650  $\text{cm}^{-1}$  stretching frequency range. The solvent-induced O–H stretching frequency shift follows a linear relationship with the solvent polarity function  $F_0 = (2\epsilon_0 - 2)/(2\epsilon_0 + 1)$ , where  $\epsilon_0$  is the static dielectric constant of the solvent, as well as the well-known correlation between O–H stretching vibrations and hydrogen bond structure for hydrogen-bonded complexes in the electronic ground state.

We have calculated O–H stretching frequencies, based on (time-dependent) density functional theory (TD-)DFT/B3LYP level with the TZVP basis sets, including solute–solvent couplings described by the standard polarizable continuum model (IEF-PCM). Comparisons to the corresponding results obtained with explicit expressions for solvent-induced vibrational frequency shifts based on the Pullin perturbative approach for solute–solvent couplings including dynamical dielectric effects show that the Pullin model provides a description of solvatochromic effects in closer agreement with experimental data. The Pullin model makes a more accurate comparison to experiment than the tested PCM model, and is

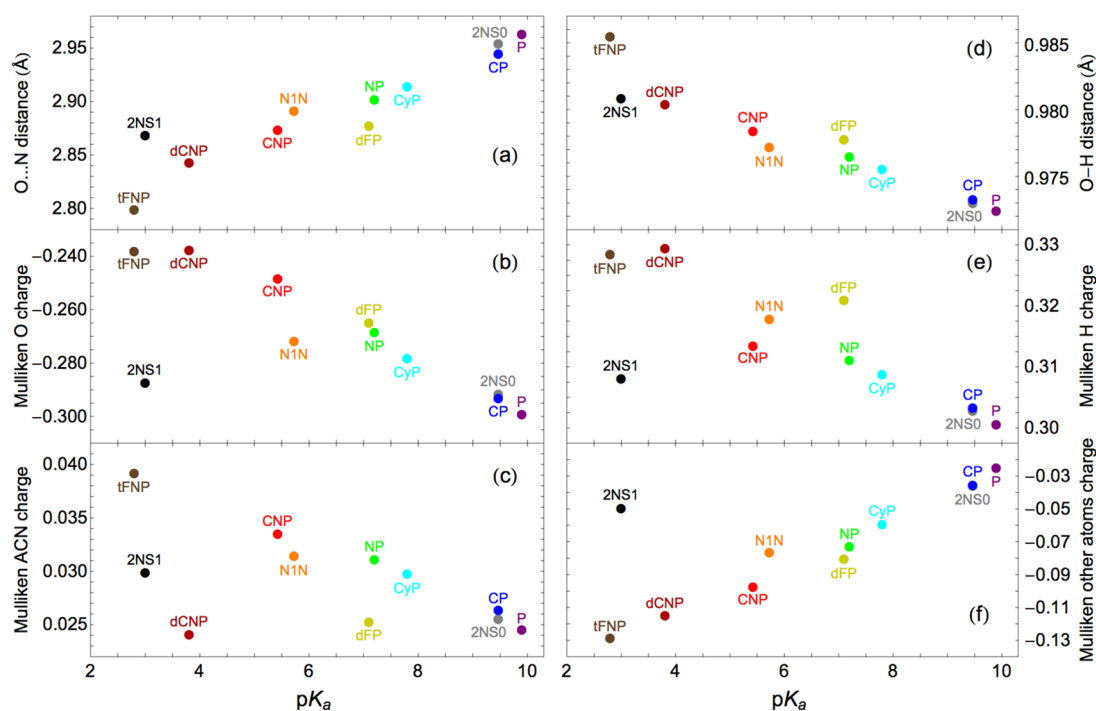


**Figure 8.** Dependence of (a) the calculated O...N distance, (b) the calculated O–H distance, (c) the gas phase Mulliken charges for the alcohol oxygen atom, and (d) the gas phase Mulliken charges for the alcohol hydrogen atom on the measured  $pK_a$  for each uncomplexed species in aqueous solution for each complex. Calculated sums of Mulliken charges of the acetonitrile base (e) and the remaining aromatic ring system, including the other substituents (f), are shown for comparison as well.

recommended if computational resources allow for gas phase anharmonic frequency calculations on a given system.

We find clear trends correlating vibrational frequency shifts with the electronic and hydrogen-bonded structure of aromatic alcohol-CH<sub>3</sub>CN complexes. We estimated the O–H stretching frequency of the corresponding hydrogen-bonded complexes in the gas-phase from the intercept at  $F_0 = 0$  ( $\epsilon_0 = 1$ ) of the vibrational frequency plot as a function of  $F_0$  and we find it is directly correlated with the O...N and O–H hydrogen-bond distances. Therefore, the O–H stretching is a direct local probe of hydrogen-bond strength that follows the acidity trends of aromatic alcohols as indicated by reported  $pK_a$  values. The slopes in the solvent-induced O–H stretching frequency plots follow similar trends, albeit with larger deviations with microscopic origin. For example, ortho-substituted aromatic alcohols have different values of the slope due to steric hindrance effects.

Our implementation of the solute–solvent couplings allows for a determination of the impact of the polar solvent dielectric on the hydrogen bond structure. Comparing the results for the nonpolar and most polar cases used in this study (*n*-hexane vs acetonitrile) leads to the conclusion that the differences in charge distribution for these two solvents are about an order of magnitude smaller than the difference between the strongest and the weakest acid used in our study.

We find that photoexcitation of 2N increases the acidity of the OH group within the range of acidity shifts typically induced by substituent groups in the aromatic ring. Upon electronic excitation, the hydrogen bond is slightly strengthened, the O...N distance contracts by 3% and the O–H distance increases by only 0.8%. The atomic charges of the OH group confirm previous reports indicating that electronic excitation affects the charge distribution of the photoacid side in the Förster cycle.

The most important finding is that for our investigated set of aromatic alcohol-acetonitrile hydrogen-bonded complexes there is an intimate correlation between the O–H stretching marker mode and the acid–base chemical reactivity. The underlying reason is that the O–H stretching frequency is a direct probe of the hydrogen bond strength as influenced by the solvation effects of the dielectric environment. Hydrogen bond structure also dictates the potential energy curves for the proton transfer coordinate, and is thus correlated with acid reactivity. Our results are thus in accordance with the general empirical finding that thermodynamic properties (acidity, proton transfer reactivity as indicated through the  $pK_a$  values determined in water) correlate well with both spectroscopic observables (the frequency shift of the O–H stretching marker mode) and hydrogen bond strengths (i.e., the hydrogen bond distances).<sup>4</sup> The validity of these general empirical correlations between acidity, spectral shifts of molecular transitions, and hydrogen bond distances may be tested further by studying a larger range of acidities of hydrogen bonded molecular acids, including a detailed survey of the impact of other media.<sup>78,79</sup> It is well-known that photoacids can be used as tools to probe local *pH* conditions. Our findings show the potential of using the O–H stretching mode as a local marker of transient hydrogen-bond structure. Performing a complementary study, taking one particular photoacid and a collection of bases, and investigating the O–H stretching frequency shift dependence as a function of the basicity of the attached base, would elucidate even more this intimate connection between the O–H stretching marker mode, hydrogen-bond structure and acid–base reactivity. Elucidating the role of the conjugate photobase-conjugate acid states,<sup>80</sup> and the solvent couplings will be another important issue to consider in future studies. A challenge will be to extend this research to situations where the photoacid, embedded in a well-defined biological environment, is exploited

to determine the local acid–base reactivity at the active site of a protein. Probing the frequency positions of both the ground and electronic excited state configurations of a photoacid hydrogen-bonded to a basic reactive site enables grasping information on the local hydrogen-bond structure, and—thus—local acidity/basicity at the reactive site of the protein. In such a reactive site, one may anticipate more involved dynamics of the response to electronic excitation on a broader range of time scales than those of the 2-naphthol–acetonitrile complexes investigated in the current study.

## ■ ASSOCIATED CONTENT

### 📄 Supporting Information

(a) Full listing of refs 60 and 79; (b) details on synthesis of tFNP; (c) FT-IR spectra of aromatic alcohols hydrogen-bonded to acetonitrile in different solvents; (d) comparison of experiment and theory of 2N-complexes in the  $S_0$  and  ${}^1L_b$  states in the gas phase; (e) intercept and O–H stretching frequency vs O–H distance plots; (f) oxygen and hydrogen atom Mulliken charge vs solvent polarity plots; and (g) additional tables of calculated charge distributions. This material is available free of charge via the Internet at <http://pubs.acs.org>.

## ■ AUTHOR INFORMATION

### Corresponding Authors

\*E-mail: [nibberin@mbi-berlin.de](mailto:nibberin@mbi-berlin.de) (E.T.J.N).

\*E-mail: [victor.batista@yale.edu](mailto:victor.batista@yale.edu) (V.S.B).

### Notes

The authors declare no competing financial interest.

## ■ ACKNOWLEDGMENTS

The authors cordially thank Junming Ho for providing useful insight regarding implicit solvation models, and Ehud and Dina Pines, as well as Phil Kiefer and Casey Hynes, for enlightening discussions. V.S.B. acknowledges support from the National Science Foundation (NSF) Grant CHE 1213742 and super-computer time from NERSC and the Yale University Faculty of Arts and Sciences High Performance Computing Center partially funded by the NSF Grant CNS 08-21132. E.T.J.N. acknowledges support from the German Science Foundation (Project Nr. DFG - NI 492/11-1).

## ■ REFERENCES

- (1) Jeffrey, G. A.; Saenger, W. *Hydrogen Bonding in Biological Structures*; Study ed.; Springer-Verlag: Berlin and New York, 1994.
- (2) Kebarle, P. Ion Thermochemistry and Solvation from Gas-Phase Ion Equilibria. *Annu. Rev. Phys. Chem.* **1977**, *28*, 445–476.
- (3) Steiner, T. The Hydrogen Bond in the Solid State. *Angew. Chem., Int. Ed.* **2002**, *41*, 49–76.
- (4) Gilli, G.; Gilli, P. *The Nature of the Hydrogen Bond: Outline of a Comprehensive Hydrogen Bond Theory*; Oxford University Press: Oxford, U.K., and New York, 2009.
- (5) Schuster, P.; Zundel, G.; Sandorfy, C. *Vibrational Spectroscopy of the Hydrogen Bond. In The Hydrogen Bond: Recent Developments in Theory and Experiments*; North-Holland Pub. Co. and American Elsevier Pub. Co.: Amsterdam and New York, 1976.
- (6) Smirnov, S. N.; Golubev, N. S.; Denisov, G. S.; Benedict, H.; Shah-Mohammed, P.; Limbach, H. H. Hydrogen Deuterium Isotope Effects on the NMR Chemical Shifts and Geometries of Intermolecular Low-Barrier Hydrogen-Bonded Complexes. *J. Am. Chem. Soc.* **1996**, *118*, 4094–4101.
- (7) Limbach, H. H.; Tolstoy, P. M.; Perez-Hernandez, N.; Guo, J.; Shenderovich, I. G.; Denisov, G. S. OHO Hydrogen Bond Geometries

and NMR Chemical Shifts: From Equilibrium Structures to Geometric H/D Isotope Effects, with Applications for Water, Protonated Water, and Compressed Ice. *Isr. J. Chem.* **2009**, *49*, 199–216.

(8) Novak, A. Hydrogen Bonding in Solids Correlation of Spectroscopic and Crystallographic Data. In *Large Molecules: Hydrogen Bonding in Solids. Correlation of Spectroscopic and Crystallographic Data*; Springer: Berlin and Heidelberg, Germany, 1974; Vol. 18, p 177–216.

(9) Lautié, A.; Froment, F.; Novak, A. Relationship between NH Stretching Frequencies and N···O Distances of Crystals Containing NH···O Hydrogen-Bonds. *Spectrosc. Lett.* **1976**, *9*, 289–299.

(10) Mikenda, W. Stretching Frequency Versus Bond Distance Correlation of O-D(H)···Y (Y = N, O, S, Se, Cl, Br, I) Hydrogen-Bonds in Solid Hydrates. *J. Mol. Struct.* **1986**, *147*, 1–15.

(11) Mikenda, W.; Steinböck, S. Stretching Frequency vs Bond Distance Correlation of Hydrogen Bonds in Solid Hydrates: A Generalized Correlation Function. *J. Mol. Struct.* **1996**, *384*, 159–163.

(12) Libowitzky, E. Correlation of O–H Stretching Frequencies and O–H···O Hydrogen Bond Lengths in Minerals. *Monatsh. Chem.* **1999**, *130*, 1047–1059.

(13) Zewail, A. H. Four-Dimensional Electron Microscopy. *Science* **2010**, *328*, 187–193.

(14) Miller, R. J. D. Mapping Atomic Motions with Ultrabright Electrons: The Chemists' Gedanken Experiment Enters the Lab Frame. *Annu. Rev. Phys. Chem.* **2014**, *65*, 583–604.

(15) Nibbering, E. T. J.; Fidler, H.; Pines, E. Ultrafast Chemistry: Using Time-Resolved Vibrational Spectroscopy for Interrogation of Structural Dynamics. *Annu. Rev. Phys. Chem.* **2005**, *56*, 337–367.

(16) Hammes-Schiffer, S.; Stuchebrukhov, A. A. Theory of Coupled Electron and Proton Transfer Reactions. *Chem. Rev.* **2010**, *110*, 6939–6960.

(17) Rosspeintner, A.; Lang, B.; Vauthey, E. Ultrafast Photochemistry in Liquids. *Annu. Rev. Phys. Chem.* **2013**, *64*, 247–271.

(18) Pines, E.; Huppert, D.; Agmon, N. Geminate Recombination in Excited-State Proton-Transfer Reactions - Numerical-Solution of the Debye-Smoluchowski Equation with Backreaction and Comparison with Experimental Results. *J. Chem. Phys.* **1988**, *88*, 5620–5630.

(19) Pines, E.; Manes, B. Z.; Lang, M. J.; Fleming, G. R. Direct Measurement of Intrinsic Proton Transfer Rates in Diffusion-Controlled Reactions. *Chem. Phys. Lett.* **1997**, *281*, 413–420.

(20) Rini, M.; Magnes, B. Z.; Pines, E.; Nibbering, E. T. J. Real-Time Observation of Bimodal Proton Transfer in Acid-Base Pairs in Water. *Science* **2003**, *301*, 349–352.

(21) Perez-Lustres, J. L.; Rodriguez-Prieto, F.; Mosquera, M.; Senyushkina, T. A.; Ernsting, N. P.; Kovalenko, S. A. Ultrafast Proton Transfer to Solvent: Molecularity and Intermediates from Solvation- and Diffusion-Controlled Regimes. *J. Am. Chem. Soc.* **2007**, *129*, 5408–5418.

(22) Simkovitch, R.; Karton-Lifshin, N.; Shomer, S.; Shabat, D.; Huppert, D. Ultrafast Excited-State Proton Transfer to the Solvent Occurs on a Hundred-Femtosecond Time-Scale. *J. Phys. Chem. A* **2013**, *117*, 3405–3413.

(23) Pines, E.; Pines, D. Proton Dissociation and Solute-Solvent Interactions Following Electronic Excitation of Photoacids. In *Ultrafast Hydrogen Bonding Dynamics and Proton Transfer Processes in the Condensed Phase*; Eisaesser, T., Bakker, H. J.; Understanding Chemical Reactivity 23; Springer Science+Business Media: Dordrecht, The Netherlands, 2002; pp 155–184

(24) Tolbert, L. M.; Solntsev, K. M. Excited-State Proton Transfer: From Constrained Systems to “Super” Photoacids to Superfast Proton Transfer. *Acc. Chem. Res.* **2002**, *35*, 19–27.

(25) Kohen, A.; Limbach, H.-H. The Kinetic Isotope Effect in the Photo-Dissociation Reaction of Excited-State Acids in Aqueous Solutions. In *Isotope effects in chemistry and biology*; Taylor & Francis: Boca Raton, FL, 2006; p 451–464.

(26) Prémont-Schwarz, M.; Barak, T.; Pines, D.; Nibbering, E. T. J.; Pines, E. Ultrafast Excited-State Proton-Transfer Reaction of 1-Naphthol-3,6-Disulfonate and Several 5-Substituted 1-Naphthol Derivatives. *J. Phys. Chem. B* **2013**, *117*, 4594–4603.

- (27) Mohammed, O. F.; Pines, D.; Dreyer, J.; Pines, E.; Nibbering, E. T. J. Sequential Proton Transfer Through Water Bridges in Acid-Base Reactions. *Science* **2005**, *310*, 83–86.
- (28) Mohammed, O. F.; Pines, D.; Nibbering, E. T. J.; Pines, E. Base-Induced Solvent Switches in Acid-Base Reactions. *Angew. Chem., Int. Ed.* **2007**, *46*, 1458–1461.
- (29) Cox, M. J.; Bakker, H. J. Parallel Proton Transfer Pathways in Aqueous Acid-Base Reactions. *J. Chem. Phys.* **2008**, *128*, 174501–10.
- (30) Granucci, G.; Hynes, J. T.; Millié, P.; Tran-Thi, T.-H. A Theoretical Investigation of Excited-State Acidity of Phenol and Cyanophenols. *J. Am. Chem. Soc.* **2000**, *122*, 12243–12253.
- (31) Hynes, J. T.; Tran-Thi, T.-H.; Granucci, G. Intermolecular Photochemical Proton Transfer in Solution: New Insights and Perspectives. *J. Photochem. Photobiol. A* **2002**, *154*, 3–11.
- (32) Tran-Thi, T.-H.; Prayer, C.; Millié, P.; Uznanski, P.; Hynes, J. T. Substituent and Solvent Effects on the Nature of the Transitions of Pyrenol and Pyranine. Identification of an Intermediate in the Excited-State Proton-Transfer Reaction. *J. Phys. Chem. A* **2002**, *106*, 2244–2255.
- (33) Matsumoto, Y.; Ebata, T.; Mikami, N. Characterizations of the Hydrogen-Bond Structures of 2-naphthol-(H<sub>2</sub>O)(*n*), (*n* = 0–3 and 5) Clusters by Infrared-Ultraviolet Double-Resonance Spectroscopy. *J. Chem. Phys.* **1998**, *109*, 6303–6311.
- (34) Matsumoto, Y.; Ebata, T.; Mikami, N. Photofragment-Detected IR Spectroscopy (PFDIRS) for the OH Stretching Vibration of the Hydrogen-Bonded Clusters in the S-1 State - Application to 2-naphthol-B (B = H<sub>2</sub>O and CH<sub>3</sub>OH) Clusters. *J. Phys. Chem. A* **2001**, *105*, 5727–5730.
- (35) David, O.; Dedonder-Lardeux, C.; Jouvet, C. Is There an Excited State Proton Transfer in Phenol (or 1-naphthol)-Ammonia Clusters? Hydrogen Detachment and Transfer to Solvent: A Key for Non-Radiative Processes in Clusters. *Int. Rev. Phys. Chem.* **2002**, *21*, 499–523.
- (36) Manca, C.; Tanner, C.; Leutwyler, S. Excited state hydrogen atom transfer in ammonia-wire and water-wire clusters. *Int. Rev. Phys. Chem.* **2005**, *24*, 457–488.
- (37) Kouyama, K.; Miyazaki, M.; Mikami, N.; Ebata, T. IR Laser Manipulation of Cis  $\leftrightarrow$  Trans Isomerization of 2-naphthol and its Hydrogen-Bonded Clusters. *J. Chem. Phys.* **2006**, *124*, 054315–8.
- (38) Fleisher, A. J.; Morgan, P. J.; Pratt, D. W. Charge Transfer by Electronic Excitation: Direct Measurement by High Resolution Spectroscopy in the Gas Phase. *J. Chem. Phys.* **2009**, *131*, 211101–4.
- (39) Agmon, N.; Rettig, W.; Groth, C. Electronic Determinants of Photoacidity in Cyanonaphthols. *J. Am. Chem. Soc.* **2002**, *124*, 1089–1096.
- (40) Emmeluth, C.; Suhm, M. A.; Luckhaus, D. A Monomers-in-Dimers Model for Carboxylic Acid Dimers. *J. Chem. Phys.* **2003**, *118*, 2242–2255.
- (41) Heyne, K.; Huse, N.; Dreyer, J.; Nibbering, E. T. J.; Elsaesser, T.; Mukamel, S. Coherent Low-Frequency Motions of Hydrogen Bonded Acetic Acid Dimers in the Liquid Phase. *J. Chem. Phys.* **2004**, *121*, 902–913.
- (42) Dreyer, J. Hydrogen-Bonded Acetic Acid Dimers: Anharmonic Coupling and Linear Infrared Spectra Studied with Density-Functional Theory. *J. Chem. Phys.* **2005**, *122*, 184306–10.
- (43) Huse, N.; Bruner, B. D.; Cowan, M. L.; Dreyer, J.; Nibbering, E. T. J.; Miller, R. J. D.; Elsaesser, T. Anharmonic Couplings Underlying the Ultrafast Vibrational Dynamics of Hydrogen Bonds in Liquids. *Phys. Rev. Lett.* **2005**, *95*, 147402–4.
- (44) Dwyer, J. R.; Dreyer, J.; Nibbering, E. T. J.; Elsaesser, T. Ultrafast Dynamics of Vibrational N-H Stretching Excitations in the 7-azaindole Dimer. *Chem. Phys. Lett.* **2006**, *432*, 146–151.
- (45) Dreyer, J. Unraveling the Structure of Hydrogen Bond Stretching Mode Infrared Absorption Bands: An Anharmonic Density Functional Theory Study on 7-azaindole Dimers. *J. Chem. Phys.* **2007**, *127*, 054309–8.
- (46) Wassermann, T. N.; Rice, C. A.; Suhm, M. A.; Luckhaus, D. Hydrogen Bonding Lights up Overtones in Pyrazoles. *J. Chem. Phys.* **2007**, *127*, 234309–9.
- (47) Szyz, Ł.; Guo, J.; Yang, M.; Dreyer, J.; Tolstoy, P. M.; Nibbering, E. T. J.; Czarnik-Matusewicz, B.; Elsaesser, T.; Limbach, H.-H. The Hydrogen-Bonded 2-Pyridone Dimer Model System. 1. Combined NMR and FT-IR Spectroscopy Study. *J. Phys. Chem. A* **2010**, *114*, 7749–7760.
- (48) Greve, C.; Nibbering, E. T. J.; Fiddler, H. Hydrogen-Bonding-Induced Enhancement of Fermi Resonances: A Linear IR and Nonlinear 2D-IR Study of Aniline-d<sub>5</sub>. *J. Phys. Chem. B* **2013**, *117*, 15843–15855.
- (49) Buckingham, A. D. Solvent Effects in Infra-red Spectroscopy. *Proc. R. Soc. London, Ser. A* **1958**, *248*, 169–182.
- (50) Pullin, A. D. E. The Variation of Infra-red Vibration Frequencies with Solvent. *Spectrochim. Acta* **1958**, *13*, 125–138.
- (51) Pullin, A. D. E. A Theory of Solvent Effects in Infra-red Spectra. *Proc. R. Soc. London, Ser. A* **1960**, *255*, 39–43.
- (52) Prémont-Schwarz, M.; Xiao, D. Q.; Batista, V. S.; Nibbering, E. T. J. The O-H Stretching Mode of a Prototypical Photoacid as a Local Dielectric Probe. *J. Phys. Chem. A* **2011**, *115*, 10511–10516.
- (53) Xiao, D. Q.; Prémont-Schwarz, M.; Nibbering, E. T. J.; Batista, V. S. Ultrafast Vibrational Frequency Shifts Induced by Electronic Excitations: Naphthols in Low Dielectric Media. *J. Phys. Chem. A* **2012**, *116*, 2775–2790.
- (54) Messina, F.; Prémont-Schwarz, M.; Braem, O.; Xiao, D. Q.; Batista, V. S.; Nibbering, E. T. J.; Chergui, M. Ultrafast Solvent-Assisted Electronic Level Crossing in 1-Naphthol. *Angew. Chem., Int. Ed.* **2013**, *52*, 6871–6875.
- (55) Vosko, S. H.; Wilk, L.; Nusair, M. Accurate Spin-Dependent Electron Liquid Correlation Energies for Local Spin-Density Calculations - A Critical Analysis. *Can. J. Phys.* **1980**, *58*, 1200–1211.
- (56) Lee, C. T.; Yang, W. T.; Parr, R. G. Development of the Colle-Salvetti Correlation-Energy Formula into a Functional of the Electron-Density. *Phys. Rev. B* **1988**, *37*, 785–789.
- (57) Becke, A. D. Density-Functional Thermochemistry. III. The Role of Exact Exchange. *J. Chem. Phys.* **1993**, *98*, 5648–5652.
- (58) Stephens, P. J.; Devlin, F. J.; Chabalowski, C. F.; Frisch, M. J. Ab-Initio Calculation of Vibrational Absorption and Circular-Dichroism Spectra using Density-Functional Force-Fields. *J. Phys. Chem.* **1994**, *98*, 11623–11627.
- (59) Schafer, A.; Huber, C.; Ahlrichs, R. Fully Optimized Contracted Gaussian-Basis Sets of Triple Zeta Valence Quality for Atoms Li to Kr. *J. Chem. Phys.* **1994**, *100*, 5829–5835.
- (60) Frisch, M. J.; Trucks, G. W.; Schlegel, H. B.; Scuseria, G. E.; Robb, M. A.; Cheeseman, J. R.; Scalmani, G.; Barone, V.; Mennucci, B.; Petersson, G. A., et al. *Gaussian 09*, rev. C.01; Gaussian Inc.: Wallingford, CT, 2010.
- (61) Luber, S.; Adamczyk, K.; Nibbering, E. T. J.; Batista, V. S. Photoinduced Proton Coupled Electron Transfer in 2-(2'-Hydroxyphenyl)-Benzothiazole. *J. Phys. Chem. A* **2013**, *117*, 5269–5279.
- (62) Furche, F.; Ahlrichs, R. Adiabatic Time-Dependent Density Functional Methods for Excited State Properties. *J. Chem. Phys.* **2002**, *117*, 7433–7447.
- (63) Scalmani, G.; Frisch, M. J.; Mennucci, B.; Tomasi, J.; Cammi, R.; Barone, V. Geometries and Properties of Excited States in the Gas Phase and in Solution: Theory and Application of a Time-Dependent Density Functional Theory polarizable continuum model. *J. Chem. Phys.* **2006**, *124*, 094107–15.
- (64) Cancès, E.; Mennucci, B.; Tomasi, J. A New Integral Equation Formalism for the Polarizable Continuum Model: Theoretical Background and Applications to Isotropic and Anisotropic Dielectrics. *J. Chem. Phys.* **1997**, *107*, 3032–3041.
- (65) Mennucci, B.; Tomasi, J. Continuum Solvation Models: A New Approach to the Problem of Solute's Charge Distribution and Cavity Boundaries. *J. Chem. Phys.* **1997**, *106*, 5151–5158.
- (66) Cossi, M.; Barone, V.; Mennucci, B.; Tomasi, J. Ab Initio Study of Ionic Solutions by a Polarizable Continuum Dielectric Model. *Chem. Phys. Lett.* **1998**, *286*, 253–260.
- (67) Scalmani, G.; Frisch, M. J. Continuous Surface Charge Polarizable Continuum Models of Solvation. I. General Formalism. *J. Chem. Phys.* **2010**, *132*, 114110–15.

(68) Pliego, J. R.; Riveros, J. M. Parametrization of the PCM Model for Calculating Solvation Free Energy of Anions in Dimethyl Sulfoxide Solutions. *Chem. Phys. Lett.* **2002**, *355*, 543–546.

(69) Ho, J. M. Predicting pK(a) in Implicit Solvents: Current Status and Future Directions. *Aust. J. Chem.* **2014**, *67*, 1441–1460.

(70) Gryn'ova, G.; Barakat, J. M.; Blinco, J. P.; Bottle, S. E.; Coote, M. L. Computational Design of Cyclic Nitroxides as Efficient Redox Mediators for Dye-Sensitized Solar Cells. *Chem.—Eur. J.* **2012**, *18*, 7582–7593.

(71) Mulliken, R. S. Electronic Population Analysis on LCAO-MO Molecular Wave Functions. I. *J. Chem. Phys.* **1955**, *23*, 1833–1840.

(72) Scott, A. P.; Radom, L. Harmonic Vibrational Frequencies: An Evaluation of Hartree-Fock, Möller-Plesset, Quadratic Configuration Interaction, Density Functional Theory, and Semiempirical Scale Factors. *J. Phys. Chem.* **1996**, *100*, 16502–16513.

(73) Halls, M. D.; Velkovski, J.; Schlegel, H. B. Harmonic frequency Scaling Factors for Hartree-Fock, S-VWN, B-LYP, B3-LYP, B3-PW91 and MP2 with the Sadlej pVTZ Electric Property Basis Set. *Theor. Chem. Acc.* **2001**, *105*, 413–421.

(74) Merrick, J. P.; Moran, D.; Radom, L. An Evaluation of Harmonic Vibrational Frequency Scale Factors. *J. Phys. Chem. A* **2007**, *111*, 11683–11700.

(75) van der Zwan, G.; Hynes, J. T. Time-Dependent Fluorescence Solvent Shifts, Dielectric Friction, and Nonequilibrium Solvation in Polar-Solvents. *J. Phys. Chem.* **1985**, *89*, 4181–4188.

(76) Chudoba, C.; Nibbering, E. T. J.; Elsaesser, T. Site-Specific Excited-State Solute-Solvent Interactions Probed by Femtosecond Vibrational Spectroscopy. *Phys. Rev. Lett.* **1998**, *81*, 3010–3013.

(77) Nibbering, E. T. J.; Chudoba, C.; Elsaesser, T. Hydrogen-Bond Dynamics and Solvation of Electronically Excited States as Determined by Femtosecond Vibrational Spectroscopy. *Isr. J. Chem.* **1999**, *39*, 333–346.

(78) Himmel, D.; Goll, S. K.; Leito, I.; Krossing, I. A Unified pH Scale for All Phases. *Angew. Chem. Int. Ed.* **2010**, *49*, 6885–6888.

(79) Raamat, E.; Kaupmees, K.; Ovsjannikov, G.; Trummal, A.; Kutt, A.; Saame, J.; Koppel, I.; Kaljurand, I.; Lipping, L.; Rodima, T.; et al. Acidities of Strong Neutral Bronsted Acids in Different Media. *J. Phys. Org. Chem.* **2013**, *26*, 162–170.

(80) Kiefer, P. M.; Hynes, J. T. Theoretical Aspects of Tunneling Proton Transfer Reactions in a Polar Environment. *J. Phys. Org. Chem.* **2010**, *23*, 632–646.

(81) Ireland, J. F.; Wyatt, P. A. H.; Gold, V. *Adv. Phys. Org. Chem.* **1976**, *12*, 131.

(82) Sigala, P. A.; Kraut, D. A.; Caaveiro, J. M. M.; Pybus, B.; Ruben, E. A.; Ringe, D.; Petsko, G. A.; Herschlag, D. Testing Geometrical Discrimination within an Enzyme Active Site: Constrained Hydrogen Bonding in the Ketosteroid Isomerase Oxyanion Hole. *J. Am. Chem. Soc.* **2008**, *130*, 13696–13708.

(83) Creamer, L. K.; Packer, J.; Vaughan, J.; Fischer, A.; Richards, R. B.; Mann, B. R. Resonance Interactions in Naphthalene Derivatives - Dissociation of Substituted Naphthols and Naphthoic Acids. *J. Org. Chem.* **1961**, *26*, 3148–3152.

(84) Bower, V. E.; Robinson, R. A. The Ionization Constants of 2-Chloro-4-Nitrophenol and 2-Nitro-4-Chlorophenol. *J. Phys. Chem.* **1960**, *64*, 1078–1079.

(85) Serjeant, E. P.; Dempsey, B. *Ionisation Constants of Organic Acids in Aqueous Solution*; Pergamon Press: Oxford, U.K., and New York, 1979.